Eur. Phys. J. D (2024)78:37
https://doi.org/10.1140/epjd/s10053-024-00810-0

THE EUROPEAN PHYSICAL JOURNAL D

Regular Article - Atomic Physics

# Many-body theory calculations of positron binding to hydrogen cyanide

Jaroslav Hofierka[a], Brian Cunningham, and Dermot G. Green[b]

School of Mathematics and Physics, Queen's University Belfast, University Road, Belfast, Northern Ireland BT7 1NN, UK

Received 25 October 2023 / Accepted 28 January 2024


**Abstract.** Positron bound state properties in hydrogen cyanide are studied via many-body theory calculations that account for strong positron-electron correlations including positron-induced polarization, screening of the electron–positron Coulomb interaction, virtual-positronium formation and positron–hole repulsion. Specifically, the Dyson equation is solved using a Gaussian basis, with the positron self-energy in the field of the molecule calculated using the Bethe–Salpeter equations for the two-particle and particle–hole propagators. The present results suggest near cancellation of screening corrections to the bare polarization, and the non-negligible role of the positron–hole interaction. There are no existing measurements to compare to for HCN. Previous configuration interaction (CI) and fixed-node diffusion Monte Carlo (FN-DMC) calculations give positron binding energies in the range 35–44 meV, most of which used a single even-tempered basis centred near the nitrogen atom. Using a similar single-centre positron basis we calculate a positron binding energy of 41 meV, in good agreement. However, we find that including additional basis centres gives an improved description of the positron wave function near the nuclei, and results in a converged binding energy in the range 63–73 meV (depending on geometry and approximation to the positron–molecule correlation potential used).

## 1 Introduction

Positrons are unique probes of matter, with applications in materials science (ultra-sensitive diagnostic studies of surfaces, defects and porosity) [1], medical imaging (PET) [2–7], astrophysics [8–11], molecular spectroscopy [12–14], and creation of positronium and antihydrogen for tests of fundamental physics including gravity (see e.g., [15–25]).

Positron interactions with matter are characterized by strong many-body correlations. They significantly modify scattering, enhance annihilation rates by orders of magnitudes (see [12] for a review), and lead to positron binding in atoms and molecules [12,26–32]. They also make the theoretical description of positron-matter interactions very challenging. Whilst positron binding energies have to date been measured for over 90 molecules (via vibrational-Feshbach resonant annihilation spectra) [12,33–41], it was only recently that we developed a many-body theory approach that provided the first *ab initio* calculated binding energies in agreement with experiment (for a handful of polar and non-polar molecules) [32,42]. We have since extended the method to successfully describe positron annihilation on the small non-binding molecules $H_2$, $N_2$ and $CH_4$ [43], and positronic bonding in molecular dianions [44].

In this paper, we apply the many-body approach to investigate positron binding to hydrogen cyanide (HCN). This molecule has a substantial dipole moment of about 3 D [45] meaning that positron binding happens even at the mean-field HF level of theory.[1] Whilst we are not aware of any reported experimental results to date, previous *ab initio* calculations of the HCN positron binding energy have been carried out using the Hartree-Fock (HF), Configuration Interaction (CI), and diffusion Monte Carlo (DMC) methods. The CI calculations [47–49] reported binding energies $\varepsilon_b = 35$, 40, and 44 meV, using different Gaussian basis sets with a limited number of positron basis functions, with configurational state functions limited to ground state, single excitations and electron-positron double excitations. The DMC calculations [50] produced the result of $\varepsilon_b = 38 \pm 5$ meV. As CI and DMC are variational methods, their predictions should be considered as lower bounds on the true binding energy. Notably, the calculations of [48–50] all employed a single positron basis centre (close to the nitrogen atom) to expand the positron wave function, and it is known that the CI expansion

[a] e-mail: jhofierka01@qub.ac.uk (corresponding author)
[b] e-mail: d.green@qub.ac.uk (corresponding author)

[1] A polar molecule in its rotational ground state with dipole moment $\mu > 1.625$ D possesses an infinite number of positron bound states [46].

Published online: 03 April 2024

for positronic systems converges slowly [47,49]. In addition to the *ab initio* methods, a recent model-potential calculation, which assumed an isotropic dipole polarizability, found a binding energy in the range 31–81 meV (dependent on the 'cut-off parameter' used in the model potential), with a recommended value of 47 meV [51].

Using the same positron basis size as the DMC calculation, our many-body approach gives a binding energy of 41 meV, in good agreement with the DMC result of $38 \pm 5$ meV. However, we performed a basis-set sensitivity study and found that by including Gaussians on additional centres, notably the atoms of the molecule, and additional ghost centres, we obtain converged binding energy that is in the range 63–73 meV (depending on the molecular geometry, and the approximation used for the positron-molecule correlation potential). Moreover, we calculate the anisotropic dipole polarizability tensor, and find that it is highly anisotropic: the component along the molecular axis (of most importance for positron binding, see below) is about 1.3 times larger than the isotropic polarizability, explaining our relative larger binding energy compared with the isotropic-polarizability-based model-potential calculations of [51].

We present the essentials of our many-body theory method and the numerical details for the present calculations, and then discuss our binding energy and annihilation rate calculations, including considerations of basis set convergence.

## 2 Theory and numerical implementation

A comprehensive description of the many-body theory method and its implementation in our `EXCITON+` code is provided in [32], so here we give only a brief overview and detail the basis parameters used for the present calculations. We calculate the positron wave function $\psi_\epsilon$ and binding energy $\epsilon$ by solving the Dyson equation

$$\left(H^{(0)} + \hat{\Sigma}_\epsilon\right) \psi_\epsilon(\boldsymbol{r}) = \epsilon\psi_\epsilon(\boldsymbol{r}), \tag{1}$$

where $H^{(0)}$ is the zeroth-order Hamiltonian for the positron in the field of the ground-state molecule, and $\hat{\Sigma}_\epsilon$ is the positron-molecule correlation potential (irreducible self-energy, equivalent to an optical potential [52]), which is non-local and energy-dependent. For positron bound states, the latter property means the equation is to be solved self-consistently at the bound state energy $E = \epsilon_b$.

We construct the self-energy diagrammatically via its expansion in the residual electron–electron and electron–positron interactions (see Fig. 1 of Hofierka et al. [32]). Three infinite classes of diagrams are included. The first is the so-called *GW* diagram that describes the polarization of the electron cloud by the positron, and corrections to it that describe screening of the electron–positron Coulomb interaction (random phase approximation) and additional electron–hole attraction (time-dependent Hartree–Fock, or, if screened electron–hole interactions are used as done in this work, the so-called Bethe-Salpeter Equation approximation, *GW*@BSE). For the positron the *GW* diagram alone is insufficient, as one must take accurate account of strong attraction due to virtual positronium (Ps) formation (where an electron temporarily tunnels from the molecule to the positron), which is described by the diagram $\Sigma^\Gamma$ that includes the infinite ladder series of electron–positron interactions. Finally, we also consider the (screened) infinite series of positron-hole repulsive interactions $\Lambda$, which is similar to $\Gamma$ in structure. The total self-energy we consider here is the sum of the three channels $\Sigma = \Sigma^{GW+\Gamma+\Lambda}$. In practice we work with the matrix elements of $\Sigma$ in the Hartree-Fock molecular orbital (MO) basis, and construct the individual contributions to $\Sigma$ by solving the respective Bethe-Salpeter equations for the electron–hole polarization propagator $\Pi$, the two-particle electron-positron propagator $G_{\Pi}^{\mathrm{ep}}$ and the positron-hole propagator $G_{\Pi}^{\mathrm{ph}}$ [53]. Their general form is $\boldsymbol{L}(\omega) = \boldsymbol{L}^{(0)}(\omega) + \boldsymbol{L}^{(0)}(\omega)\boldsymbol{K}\boldsymbol{L}(\omega)$ where the $\boldsymbol{L}^{(0)}$ are non-interacting two-body propagators and $\boldsymbol{K}$ are the interaction kernels [53,54]. In the excitation space of pair product HF orbitals $\boldsymbol{L} = (\boldsymbol{C}\omega - \boldsymbol{H})^{-1} = \boldsymbol{\xi}(\omega - \boldsymbol{\Omega})^{-1}\boldsymbol{\xi}^{-1}\boldsymbol{C}^{-1}$, where the pair transition amplitudes $\xi$ are the solutions of the pseudo-Hermitian linear-response generalized eigenvalue equations [55–57] of the form

$$\boldsymbol{H}\boldsymbol{\xi} = \boldsymbol{C}\boldsymbol{\xi}\boldsymbol{\Omega}, \tag{2}$$

with $\boldsymbol{\xi}^\dagger\boldsymbol{C}\boldsymbol{\xi} = \boldsymbol{C}$. The explicit form of the individual matrices can be found in [32]. Here the $\boldsymbol{H}$ matrix depends on the particular two-particle propagator $\boldsymbol{L}$ under consideration and the approximation used for it (see Extended Table 4 in [32] for the explicit matrix elements), and $\boldsymbol{\xi}$ is the matrix of (de-)excitation eigenvectors $\boldsymbol{X}_n$ ($\boldsymbol{Y}_n$) with the corresponding (de-)excitation energies $\Omega_n^+$ ($\Omega_n^-$). Expanding the positron Dyson wave function (see Eq. 1) in the positron HF MO basis as $\psi_\varepsilon(\mathbf{r}) = \sum_\nu D_\nu^\varepsilon \varphi_\nu^+(\mathbf{r})$ transforms the Dyson equation to the linear matrix equation $\boldsymbol{F}\boldsymbol{D} = \boldsymbol{\varepsilon}\boldsymbol{D}$, where $\langle\nu_1|F|\nu_2\rangle = \varepsilon_{\nu_1}\delta_{\nu_1\nu_2} + \langle\nu_1|\Sigma_\varepsilon|\nu_2\rangle$.

The electron (−) and positron (+) Hartree-Fock molecular orbitals are themselves expanded in distinct Gaussian basis sets as

$$\varphi_a^\pm(\boldsymbol{r}) = \sum_A^{N_c^\pm} \sum_{k=1}^{N_A^\pm} C_{aAk}^\pm \chi_{A_k}^\pm(\boldsymbol{r}), \tag{3}$$

where $A$ labels the $N_c^\pm$ basis centres, $k$ labels the $N_A^\pm$ different Gaussians on centre $A$, each taken to be of Cartesian type with angular momentum $l^x + l^y + l^z$, such that

$$\chi_{A_k}(\boldsymbol{r}) = \mathcal{N}_{A_k}(x - x_A)^{l^x_{Ak}}(y - y_A)^{l^y_{Ak}} \times (z - z_A)^{l^z_{Ak}} e^{-\zeta_{Ak}|\mathbf{r}-\mathbf{r}_A|^2}, \quad (4)$$

where $\mathcal{N}_{A_k}$ is a normalization constant, and $C$ are the expansion coefficients determined from the solution of the Roothaan equations.

For the electrons we include aug-cc-pVQZ [58] basis sets centred on the H, C and N atoms. For the positron, we likewise place aug-cc-pVQZ basis sets on the H and C atoms, but, to capture the long-range correlation and full extent of the positron wave function,[2] We place a diffuse even-tempered Gaussian basis on the N atom of $10s9p8d7f$ form (unless otherwise stated) with exponents $\zeta_j = \zeta_1\beta^{j-1}$,with $j = 1, \ldots, N^l$, for angular momentum $l$ and parameters $\zeta_1 > 0$ and $\beta > 1$. In practice we performed binding energy calculations for a range of $\zeta_1$ and $\beta$ finding that there are broad ranges of stability. For Hartree-Fock calculations, the optimal $\beta = 3.0$ and $\zeta_1$ was set to $10^{-5}$ for $s$- and $p$-type Gaussians and $10^{-4}$ for $d$- and $f$-type Gaussians (atomic units are used throughout unless otherwise stated). For many-body theory calculations, $\beta = 2.2$ and $\zeta_1$ was $10^{-3}$ for $s$- and $p$-type Gaussians and $10^{-2}$ for $d$- and $f$-type Gaussians. It is known that the convergence of many-body theory calculations with respect to the maximal orbital angular momentum is quite slow [59] and arises from the need to describe virtual Ps localized outside the atom by an expansion in terms of single-particle orbitals centred on the nuclei. Finally, to more accurately describe virtual-Ps we place (hydrogen) aug-cc-pVQZ electron and positron basis sets on additional 'ghost' centres (up to 18) at manually optimized locations near the molecule; they generate effectively higher angular momenta basis functions (see, e.g. Appendix B in [51]).

The most computationally demanding part of our approach is in the calculation of the virtual-Ps self-energy contribution $\Sigma^\Gamma$. For this, the BSE matrix dimension is $N_\nu \times N_\mu$, the product of total number of positron and excited electron MOs. For the largest calculation considered here, which employed 18 additional ghost centres, $N_\nu = 600$ and $N_\mu = 453$, resulting in the matrix of $271,800^2$ elements, the diagonalisation of which demanded about 4.8 TB of RAM.[3]

Solution of the Dyson equation yields not only the positron binding energy but also the positron-bound state wave function $\psi_\varepsilon$. Using it, the $2\gamma$ annihilation rate in the bound state $\Gamma = \pi r_0^2 c \delta_{ep}$ ($\Gamma[\mathrm{ns}^{-1}] = 50.47\,\delta_{ep}$[a.u.]), whose inverse is the lifetime of the positron-molecule complex with respect to annihilation, can be calculated. Here $r_0$ is the classical electron radius, $c$ is the speed of light and $\delta_{ep}$ is the contact density

$$\delta_{ep} = \sum_{n=1}^{N_e} \gamma_n \int |\varphi_n(\boldsymbol{r})|^2 |\psi_\varepsilon(\boldsymbol{r})|^2 d\boldsymbol{r}, \quad (5)$$

where $\gamma_n$ are orbital dependent enhancement factors that account for the short-range electron-positron attraction [60,61]. Previous many-body calculations for atoms by one of us determined the enhancement factors to follow a physically motivated scaling with the orbital energy $\varepsilon_n$ in atomic units [60,61]

$$\gamma_n = 1 + \sqrt{1.31/|\varepsilon_n|} + (0.834/|\varepsilon_n|)^{2.15}, \quad (6)$$

which we assume to hold here.

Finally, we also calculate the dipole polarizability tensor as [62,63]

$$\alpha_{ij}(E) = 2\sum_n \Omega_n \frac{\boldsymbol{\mu}_i^T \boldsymbol{X}_n \boldsymbol{X}_n^T \boldsymbol{\mu}_j}{\Omega_n^2 - E^2}, \quad (7)$$

where $\boldsymbol{\mu}_i$ are vectors of transition dipole moment one-electron integrals for $i = x, y, z$. Note that in the HF approximation, the eigenvector matrix $\boldsymbol{X}_n$ (see above) is a unit matrix and the eigenvalues $\Omega_n$ reduce to the HF orbital energy differences. The isotropic static dipole polarizability is

$$\bar{\alpha} = \frac{1}{3}\left[\alpha_{xx}(0) + \alpha_{yy}(0) + \alpha_{zz}(0)\right]. \quad (8)$$

## 3 Results and discussion

Table 1 presents our calculated HCN positron binding energies, as well as contact densities, dipole moments, and static dipole polarizabilities, compared with earlier CI, DMC and model-potential calculations. We consider two molecular geometries: one optimized at the HF/aug-cc-pVQZ level via minimization of the total electronic HF energy using the `Molpro` [64,65] package, ensuring an internally consistent *ab initio* calculation, while the second is the experimental geometry [45]. Comparing the results obtained for the two geometries, we observe 3% increase in the C-N bond length $r_{\mathrm{CN}}$ going from HF-optimized to experimental geometry, leading to 3% change in HF binding energy but 9% difference in many-body binding energies. Further, the static dipole polarizability increases by about 4% while ionization energies decrease by about 0.3 eV. We note that the dipole moments are reported at Hartree–Fock level only, while the ionization energies and polarizabilities have been computed at both HF and *GW*-BSE levels of theory, as shown in Table 2. Table 2 lists

[2] The bound positron wave function behaves asymptotically as $\psi \propto e^{-\kappa r}$, where $\kappa = \sqrt{2\varepsilon_b}$. Thus, to ensure that the expansion describes the wave function well at $r \sim 1/\kappa$, i.e., that the broadest Gaussian covers the extent of the positron wave function, one must have $\zeta_1 \lesssim \kappa^2 = 2\varepsilon_b$.

[3] The calculations were performed in `EXCITON+` using ScaLAPACK, running on three AMD EPYC 128 CPU @ 2 GHz, 2 TB RAM nodes of the United Kingdom Tier-2 supercomputer 'Kelvin-2' at Queen's University Belfast.

**Table 1** Comparison of HCN positron binding energies $\varepsilon_b$ for optimized and experimental geometries and previously calculated results

| | $r_{\mathrm{CN}}$(Å) | $\mu$ (D) | $\alpha$ (Å$^3$) | Binding energies (meV) $\varepsilon_b^{\mathrm{HF}}$ | $\varepsilon_b^{\mathrm{BSE}}$ | $\varepsilon_b^{\mathrm{best}}$ | $\delta_{ep}$ (a.u.) |
|---|---|---|---|---|---|---|---|
| *This work* | | | | | | | |
| Opt. geom. (single $e^+$ centre) | 1.123 | 3.26 | 2.35 | 1.83 | 21 | 41, 44 | 3.0, 3.3×10$^{-3}$ |
| Opt. geom. (converged) | 1.123 | 3.26 | 2.35 | 1.89 | 23 | 63, 68 | 4.7, 5.0×10$^{-3}$ |
| Experim. geom. (converged) | 1.156 | 3.29 | 2.43 | 1.95 | 24 | 69, 73 | 5.0, 5.3×10$^{-3}$ |
| *Previous theory* | | | | | | | |
| CI [48] | 1.124 | 3.26 | – | 1.66 | – | 44 | – |
| CI [49] | 1.160 | 3.32 | 2.28 | – | – | 40 | – |
| CI [47] | 1.167 | 3.31 | 2.29 | 1.63 | – | 35 | – |
| DMC [50] | 1.167 | – | – | 2.00 | – | 38 ± 5 | – |
| Model potential [51] | 1.126 | – | 2.63 | 1.94 | – | 47 | 4.1×10$^{-3}$ |

The first row shows results for a single $e^+$ centre calculation, which used an even-tempered basis $15s15p6d2f$ on nitrogen with $\zeta_1 = 10^{-5}$ for $s$ and $p$-Gaussians, $\zeta_1 = 10^{-3}$ for $d$-Gaussians, and $\zeta_1 = 10^{-1}$ for $f$-Gaussians, with $\beta = 3.0$ in all cases. Converged calculations used 21 positron basis centres on 3 atoms and 18 ghost centres, with an even-tempered $10s9p8d7f$ basis on nitrogen and aug-cc-pVQZ basis sets on the remaining centres. Binding energies $\varepsilon_b^{\mathrm{best}}$ and positron–electron contact densities $\delta_{ep}$ are calculated at $\Sigma^{GW@\mathrm{BSE}+\tilde{\Gamma}+\tilde{\Lambda}}$ level of theory using either HF or $GW$ energies in the diagram sums (first and second number). Also shown are the C-N bond length $r_{\mathrm{CN}}$, dipole moment $\mu$, and static dipole polarizability $\alpha$. Positron-electron contact densities include the enhancement factors (Eq. 6) and the quasi-particle normalization constant $a$ (Eq. 9)

**Table 2** Calculated static dipole polarizabilities and ionization energies of HCN for optimized and experimental geometries along principal Cartesian axes (diagonal elements of the polarizability tensor) at HF and BSE levels of theory (Eq. 7) with $\bar{\alpha}$ their average

| | HF polarizability (Å$^3$) | | | | BSE polarizability (Å$^3$) | | | | | Ionization energy (eV) | | |
|---|---|---|---|---|---|---|---|---|---|---|---|---|
| | $xx$ | $yy$ | $zz$ | $\bar{\alpha}$ | $xx$ | $yy$ | $zz$ | $\bar{\alpha}$ | $\bar{\alpha}_{\mathrm{ref.}}$ | HF | $GW$ | Ref. [45] |
| Opt. geom. | 1.81 | 1.81 | 3.13 | 2.26 | 1.97 | 1.97 | 3.08 | 2.35 | – | 13.78 | 14.05 | – |
| Exp. geom. | 1.88 | 1.88 | 3.37 | 2.37 | 2.04 | 2.04 | 3.23 | 2.43 | 2.46 | 13.50 | 13.88 | 13.60 |

The reference data are from [45]

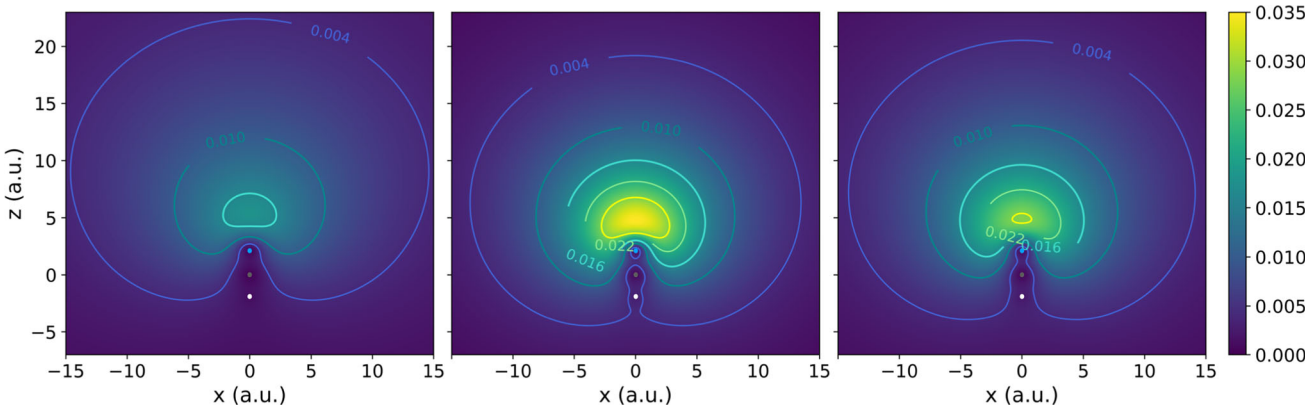


**Fig. 1** Positron bound state wave function in the $xz$ plane (with the H, C, and N atoms located at −2.00, 0, and 2.12 a.u. along the $z$ axis) for three different approximations to the positron self-energy: $\Sigma^{\mathrm{BSE}}$ (left), $\Sigma^{\mathrm{BSE}+\Gamma}$ (middle) and $\Sigma^{\mathrm{BSE}+\tilde{\Gamma}+\tilde{\Lambda}}$ (right)

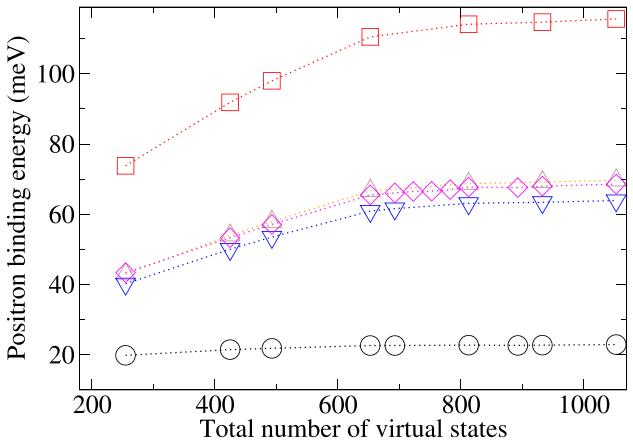


**Fig. 2** Convergence of positron binding energy with respect to the total number of positron and electron excited states included in the calculation (with the positron states accounting for about 60% of the total) for a number of different approximations to $\Sigma$: the $GW$@BSE (circles); including the virtual-Ps ladder series of screened electron-positron interactions; the $\Sigma^{\Gamma}$ (squares); and additionally the ladder series of positron-hole interactions $\Sigma^{\Lambda}$ (triangles up). Results obtained using screened Coulomb interactions in the 'Γ' and 'Λ-block' are shown as triangles down, with the additional use of $GW$ energies instead of HF ones in the diagrams leading to the results shown as diamonds

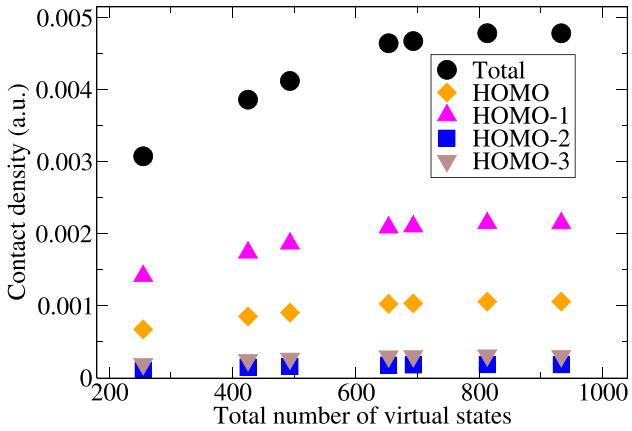


**Fig. 4** Convergence of positron-electron annihilation contact density in the bound state with respect to the total number of positron and electron excited states included in the calculation (with the positron states accounting for about 60% of the total) for the electron valence MOs of HCN (HOMO-3: triangles down, HOMO-2: squares, HOMO-1: triangles up, HOMO: diamonds, and the total sum shown as circles) with enhancement factors (see Eq. 6). Here, the positron Dyson wave function is computed at $\Sigma^{GW+\tilde{\Gamma}+\tilde{\Lambda}}$ level of theory

the main components of the static dipole polarizability tensor at both HF and $GW$-BSE levels of theory, with the molecule aligned along the $z$-axis. Regarding basis-set dependency, these values are not appreciably affected by addition of ghost basis centres, whose primary purpose is to enlarge the virtual basis space in the many-body theory calculations; e.g., dipole polarizabilities remain the same within the stated precision, while the $GW$ ionization energies fluctuate between 14.13 and 14.05 eV. As far as the experimental geometry is concerned, excellent agreement with the reference polarizability and ionization energy data is found [45].

Being a strongly polar molecule, HCN binds the positron even at the level of a static-potential approximation, with a binding energy of ∼1.89 meV and contact density $\delta_{ep}^{(0)} = 1.00 \times 10^{-5}$ a.u., in excellent agreement with the corresponding earlier HF results 1.94 meV and $0.967\times10^{-5}$ a.u. [51]. Other methods reported HF binding energies of 1.6 meV [47,48] and 2.0 meV [50] (see Table 1). Differences are due to slightly different bond lengths, basis sets, and the par-

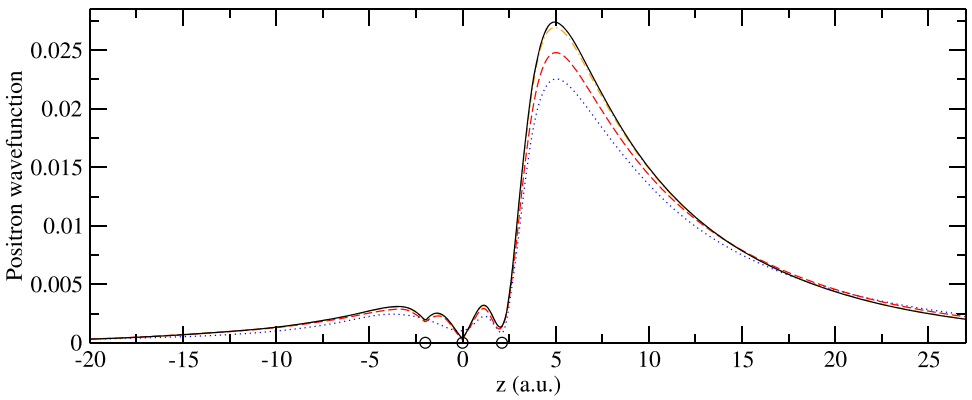


**Fig. 3** Convergence of the positron bound state wave function for HCN projected along the main symmetry axis (with H,C,N atoms indicated by circles located at −2.0, 0, and 2.12 a.u.) with respect to the basis size (represented by the number of ghost centres) at the $\Sigma^{GW+\tilde{\Gamma}+\tilde{\Lambda}}$ level of theory. The single atom basis calculation (dotted line) used a $15s15p6d2f$ positron basis on the nitrogen atom (as done in [50]), while the remaining calculations used a $10s9p8d7f$ positron basis on nitrogen and aug-cc-pVQZ basis sets on hydrogen, carbon, and ghost atoms. The dashed line corresponds to the zero ghost calculation, the dot-dashed line a calculation with 5 ghost centres, and the solid line a calculation with 14 ghost centres

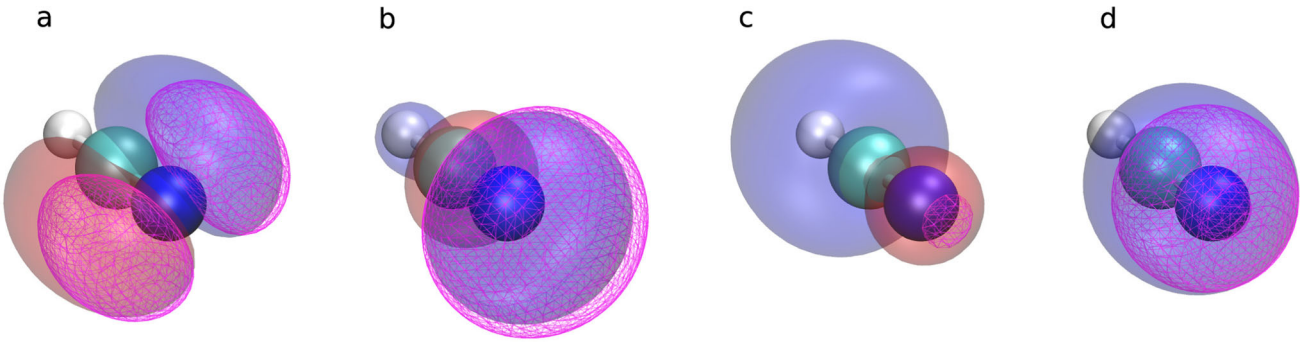


**Fig. 5** Electron valence MOs in HCN (red and blue show positive and negative electron wave function regions at ±0.006 isovalue, respectively). The highest occupied MO in (a) is doubly degenerate at 13.8 eV and has $\pi$ character while the others are $\sigma$-type with energies 15.8 eV (b), 22.1 eV (c), and 34.0 eV (d), respectively. The corresponding electron-positron contact density amplitude (magenta) is shown at the $\Sigma^{GW+\tilde{\Gamma}+\tilde{\Lambda}}$ level at 0.001 isovalue

**Table 3** Total annihilation contact density $\delta_{\rm ep}$ and fractional contribution of individual molecular orbitals, at the Hartree-Fock (HF) level of the theory and using the positron Dyson wave function either without ("unenh.") or with ("enh.") enhancement factors accounting for the short-range annihilation vertex corrections (Eq. 6)

| | HF | Dyson unenh. | Dyson enh. |
|---|---|---|---|
| Total $\delta_{\rm ep}$ | $1.00\times10^{-5}$ | $0.98\times10^{-3}$ | $4.72\times10^{-3}$ |
| HOMO | 0.19 | 0.20 | 0.22 |
| HOMO-1 | 0.44 | 0.41 | 0.45 |
| HOMO-2 | 0.05 | 0.05 | 0.04 |
| HOMO-3 | 0.11 | 0.12 | 0.06 |
| Core MOs | 0.01 | 0.02 | 0.01 |

Note that the highest occupied MO (HOMO) is doubly degenerate: the number quoted is for only one of the two contributions. Positron Dyson wave function is computed at $\Sigma^{GW+\tilde{\Gamma}+\tilde{\Lambda}}$ level of theory

ticular HF method (e.g.,"frozen target" versus "relaxed target" [51]).

Starting with the second-order $GW$ bare polarization diagram $\Sigma^{(2)}$, the HF binding energy increases substantially to $\varepsilon_b = 27$ meV. Using the RPA polarizability in the $GW$ self-energy decreases the binding energy considerably down to 7 meV. Adding in the exchange diagrams within the TDHF approximation (or RPA with exchange) increases the binding energy to 24 meV.

The inclusion of BSE screening in $GW$ diagrams reduces this slightly to 23 meV. The inclusion of the virtual-positronium block diagram $\Gamma$ increases the $GW$ binding energy by a factor of 5 (see Fig. 2) and causes the positron wave function to be strongly peaked near the nitrogen atom (see Fig. 3). Moreover, considerable positron density protrudes into the region of the HOMO $\pi$ bond, as seen in Fig. 1. Overall, the subsequent inclusion of positron-hole ladder series $\Lambda$ down by about 40% while the inclusion of screening within the rungs of the ladder diagrams is relatively less important, lowering the binding energies by 2–5% depending on the choice of SCF or $GW$ energies used in the BSE screening kernel.

It is important to note that many-body binding energies converge with the basis set size (and maximum angular momentum) significantly slower than HF binding energies, with the $\Gamma$ contribution being the slowest (see Fig. 2). We found that using up to 18 ghost atoms located 1.0 Å away from the main symmetry axis with 2 more along the axis next to nitrogen (in the region of maximum positron density, see Fig. 1) increased many-body binding energies by as much as 5% in the case of $GW$ approximation and up to 50% for the virtual-Ps level of theory results compared to a calculation with basis centres on the atoms only (see Fig. 2).

Our final converged results are higher than the previous CI [47,48] and diffusion Monte Carlo (DMC) [50] calculations by 20–30 meV. However, as CI and DMC are variational methods, their predictions should be considered as lower bounds on the true binding energy. The DMC calculation [50] employed a single even-tempered $15s15p6d2f$ positron basis centre near the nitrogen atom. Using this basis in our method, a binding energy of 41 meV was obtained, in excellent agreement with the DMC calculation (38±5 meV [50]). However, using this single-centre basis results in the positron wave function repulsion from the nuclei being poorly resolved, as shown in Fig. 3. Adding the even-tempered $10s9p8d7f$ on nitrogen and aug-cc-pVQZ basis sets on hydrogen, carbon, and ghost atoms (with the ghost atoms employing the basis of hydrogen) substantially improves the description around the atoms, and enhances the peak near the nitrogen, raising the binding energy to 63 meV. The recent model correla-

tion potential approach of Swann and Gribakin [51] produced a range of binding energies: 31, 47, and 82 meV (with corresponding contact densities equal to 2.3, 4.1, $8.6\times10^{-3}$ a.u.) obtained for cut-off radii of 2.25, 2.0, and 1.75 a.u., with smaller cut-off radii meaning a stronger correlation potential. The recommended value was 47 meV. This model potential approach assumed an isotropic molecular dipole polarizability. However, we see from Table 2 that the crucial $zz$ component of the polarizability tensor (along the molecular axis) is ∼1.3 times larger than the isotropic value. Our many-body theory approach describes the anisotropic positron-molecule potential *ab initio*. Thus the larger binding energy we find compared to the model-potential recommended value is to be expected.

The convergence of positron-electron annihilation contact density $\delta_{\rm ep}$ with the number of virtual states is shown in Fig. 4. The enhancement factors accounting for the short-range annihilation vertex corrections (Eq. 6) average to about 4.7, with the largest value of about 5.3 for the doubly degenerate HOMO decreasing with the orbital energies through 5.1 and 3.4 down to about 2.5 for the valence orbitals shown in Fig. 5. The relative contributions to the contact density of individual MOs depend on their overlaps with the positron wave function, which is affected by their shape and magnitude in the vicinity of the positron. Notably, the HOMO-1 (at 15.8 eV) contributes more to the overall contact density than HOMO, and also the HOMO-3 (at 34.0 eV) has overlap with the positron wave function than HOMO-2 (at 22.1 eV) as seen in Table 3 and Fig. 5. Finally, we note that the contact densities contain the positron Dyson wave function normalization constant

$$\int |\psi_\varepsilon(\boldsymbol{r})|^2 d\mathbf{r} = (1 - \partial\varepsilon/\partial E|_{\varepsilon_b})^{-1} \equiv a < 1, \qquad (9)$$

which estimates the degree to which the positron-molecule bound state is a single-particle state, with smaller values of $a$ signifying a more strongly-correlated state. Here we find $a = 0.986$ at the final $GW + \Gamma + \Lambda$ level of theory, mirroring the binding energies at each level of theory ($a = 0.997$ for the $GW$ level of theory, decreasing to 0.977 at $GW + \Gamma$ level).

## 4 Summary and conclusion

Many-body theory calculations of positron binding to HCN were performed using the Gaussian basis code `EXCITON+`. The effects of correlations were studied: the process of virtual-Ps formation was found to substantially enhance the binding, a near cancellation of screening corrections to the bare polarization was found, as was a non-negligible role of the positron-hole interaction. Our converged results are about 50% larger (20–30 meV in absolute terms) than previous CI or FN-DMC calculations that used a single positron basis centre. Using a similar basis we obtain results in good agreement, but find that including additional basis centres gives an improved description of the positron wave function (cusps) at the nuclei and also is required to obtain convergence of the virtual-positronium contribution to the positron-molecule correlation potential. We hope this work will stimulate further theoretical and experimental work, to shed light on this discrepancy.

**Acknowledgements** We thank Charlie Rawlins, Charles Patterson, Andrew Swann, Jack Cassidy, Sarah Gregg, and Gleb Gribakin for useful discussions, and Ian Stewart, Luis Fernandez Menchero (QUB), Martin Plummer and Alin Elena (UK STFC Scientific Computing Department) for high-performance computing assistance. This work was funded by the European Research Council grant 804383 'ANTI-ATOM'.

## Author contributions

JH performed the calculations. JH, BC and DGG wrote the `EXCITON+` code, heavily adapting the `EXCITON` code of C. H. Patterson to include positrons. DGG conceived the work. All authors contributed to the manuscript preparation.

**Funding** This work was funded by the European Research Council grant 804383 'ANTI-ATOM'.

**Data Availability Statement** This manuscript has no associated data or the data will not be deposited. All data pertaining to the results are presented within the manuscript.

**Declarations**

**Code availability** The `EXCITON+` code is available from the authors on request.

## References


1. M.J. Puska, R.M. Nieminen, Theory of positrons in solids and on solid surfaces. Rev. Mod. Phys. **66**(3), 841 (1994). https://doi.org/10.1103/RevModPhys.66.841
2. F. Blanco, A. Muñoz, D. Almeida, F. Silva, P. Limão-Vieira, M.C. Fuss, A.G. Sanz, G. García, Modelling low energy electron and positron tracks in biologically relevant media. Eur. J. Phys. D **67**(9), 199 (2013). https://doi.org/10.1140/epjd/e2013-40276-1
3. R.D. White, W. Tattersall, G. Boyle, R.E. Robson, S. Dujko, Z.L. Petrovic, A. Bankovic, M.J. Brunger, J.P. Sullivan, S.J. Buckman, G. Garcia, Low-energy electron and positron transport in gases and soft-condensed systems of biological relevance. Appl. Radiat. Isotoptopes **83**, 77–85 (2014). https://doi.org/10.1016/j.apradiso.2013.01.008
4. G.J. Boyle, W.J. Tattersall, D.G. Cocks, S. Dujko, R.D. White, Kinetic theory of positron-impact ionization in gases. Phys. Rev. A **91**, 052710 (2015). https://doi.org/10.1103/PhysRevA.91.052710
5. B. Boudaiffa, P. Cloutier, D. Hunting, M.A. Huels, L. Sanche, Resonant formation of DNA strand breaks by low-energy (3 to 20 eV) electrons. Science **287**(5458), 1658–1660 (2000). https://doi.org/10.1126/science.287.5458.1658
6. I. Baccarelli, I. Bald, F.A. Gianturco, E. Illenberger, J. Kopyra, Electron-induced damage of DNA and its components: experiments and theoretical models. Phys. Rep. **508**(1), 1–44 (2011). https://doi.org/10.1016/j.physrep.2011.06.004
7. R.L. Wahal, *Principles and Practice of Positron Emission Tomography* (Williams and Wilkins, Philadelphia, 2008)
8. N. Prantzos, C. Boehm, A. Bykov, R. Diehl, K. Ferrière, N. Guessoum, P. Jean, J. Knoedlseder, A. Marcowith, I. Moskalenko, A. Strong, G. Weidenspointner, The 511 kev emission from positron annihilation in the galaxy. Rev. Mod. Phys. **83**, 1001 (2011). https://doi.org/10.1103/RevModPhys.83.1001
9. V.V. Flambaum, I.B. Samsonov, Radiation from matter-antimatter annihilation in the quark nugget model of dark matter. Phys. Rev. D **104**, 063042 (2021). https://doi.org/10.1103/PhysRevD.104.063042
10. R. Laha, Primordial black holes as a dark matter candidate are severely constrained by the galactic center 511 kev $\gamma$-ray line. Phys. Rev. Lett. **123**, 251101 (2019). https://doi.org/10.1103/PhysRevLett.123.251101
11. C. Kierans, J.F. Beacom, S. Boggs, M. Buckley, R. Caputo, R. Crocker, M.D. Becker, R. Diehl, C.L. Fryer, S. Griffin, D. Hartmann, E. Hays, P. Jean, M.G.H. Krause, T. Linden, A. Marcowith, P. Martin, A. Moiseev, U. Oberlack, E. Orlando, F. Panther, N. Prantzos, R. Rothschild, I. Seitenzahl, C. Shrader, T. Siegert, A. Strong, J. Tomsick, W.T. Vestrand, A. Zoglauer, A. Positron Annihilation in the Galaxy. Bulletin of the AAS 51(3) (2019). https://baas.aas.org/pub/2020n3i256
12. G.F. Gribakin, J.A. Young, C.M. Surko, Positron-molecule interactions: resonant attachment, annihilation, and bound states. Rev. Mod. Phys. **82**(3), 2557 (2010). https://doi.org/10.1103/RevModPhys.82.2557
13. C.M. Surko, F.A. Gianturco (eds.), *New Directions in Antimatter Chemistry and Physics* (Springer, Berlin, 2001)
14. A.R. Swann, G.F. Gribakin, Effect of molecular constitution and conformation on positron binding and annihilation in alkanes. J. Chem. Phys. **153**(18), 184311 (2020). https://doi.org/10.1063/5.0028071
15. S.J. Brawley, S. Armitage, J. Beale, D.E. Leslie, A.I. Williams, G. Laricchia, Electron-like scattering of positronium. Science **330**(6005), 789 (2010). https://doi.org/10.1126/science.1192322
16. D.B. Cassidy, Experimental progress in positronium laser physics. Eur. J. Phys. D **72**, 53 (2018). https://doi.org/10.1140/epjd/e2018-80721-y
17. G.B. Andresen, M.D. Ashkezari, M. Baquero-Ruiz, W. Bertsche, P.D. Bowe, E. Butler, C.L. Cesar, S. Chapman, M. Charlton, A. Deller, S. Eriksson, J. Fajans, T. Friesen, M.C. Fujiwara, D.R. Gill, A. Gutierrez, J.S. Hangst, W.N. Hardy, M.E. Hayden, A.J. Humphries, R. Hydomako, M.J. Jenkins, S. Jonsell, L.V. Jørgensen, L. Kurchaninov, N. Madsen, S. Menary, P. Nolan, K. Olchanski, A. Olin, A. Povilus, P. Pusa, F. Robicheaux, E. Sarid, S.S.E. Nasr, D.M. Silveira, C. So, J.W. Storey, R.I. Thompson, D.P. Werf, J.S. Wurtele, Y. Yamazaki, Trapped antihydrogen. Nature **468**(7324), 673–676 (2010). https://doi.org/10.1038/nature09610
18. T.A. collaboration, Confinement of antihydrogen for 1,000 seconds. Nat. Phys **7**, 558–564 (2011)
19. C. Amole, M.D. Ashkezari, M. Baquero-Ruiz, W. Bertsche, E. Butler, A. Capra, C.L. Cesar, M. Charlton, S. Eriksson, J. Fajans, T. Friesen, M.C. Fujiwara, D.R. Gill, A. Gutierrez, J.S. Hangst, W.N. Hardy, M.E. Hayden, C.A. Isaac, S. Jonsell, L. Kurchaninov, A. Little, N. Madsen, J.T.K. McKenna, S. Menary, S.C. Napoli, P. Nolan, K. Olchanski, A. Olin, A. Povilus, P. Pusa, C.Ø. Rasmussen, F. Robicheaux, E. Sarid, D.M. Silveira, C. So, T.D. Tharp, R.I. Thompson, D.P. Werf, Z. Vendeiro, J.S. Wurtele, A.I. Zhmoginov, A.E. Charman, An experimental limit on the charge of antihydrogen. Nat. Commun. **5**(1), 3955 (2014). https://doi.org/10.1038/ncomms4955
20. P. Pérez, D. Banerjee, F. Biraben, D. Brook-Roberge, M. Charlton, P. Cladé, P. Comini, P. Crivelli, O. Dalkarov, P. Debu, A. Douillet, G. Dufour, P. Dupré, S. Eriksson, P. Froelich, P. Grandemange, S. Guellati, R. Guérout, J.M. Heinrich, P. Hervieux, L. Hilico, A. Husson, P. Indelicato, S. Jonsell, J. Karr, K. Khabarova, N. Kolachevsky, N. Kuroda, A. Lambrecht, A.M.M. Leite, L. Liszkay, D. Lunney, N. Madsen, G. Manfredi, B. Mansoulié, Y. Matsuda, A. Mohri, T. Mortensen, Y. Nagashima, V. Nesvizhevsky, F. Nez, C. Regenfus, J. Rey, J. Reymond, S. Reynaud, A. Rubbia, Y. Sacquin, F. Schmidt-Kaler, N. Sillitoe, M. Staszczak, C.I. Szabo-Foster, H. Torii, B. Vallage, M. Valdes, D.P. van der Werf, A. Voronin, J. Walz, S. Wolf, S. Wronka, Y. Yamazaki, The GBAR antimatter gravity experiment. Hyperfine Interact. **233**(1–3), 21–27 (2015). https://doi.org/10.1007/s10751-015-1154-8
21. C. Malbrunot, C. Amsler, S. Arguedas Cuendis, H. Breuker, P. Dupre, M. Fleck, H. Higaki, Y. Kanai, B. Kolbinger, N. Kuroda, M. Leali, V. Mäckel, V. Mascagna, O. Massiczek, Y. Matsuda, Y. Nagata, M.C. Simon, H. Spitzer, M. Tajima, S. Ulmer, L. Ven-

turelli, E. Widmann, M. Wiesinger, Y. Yamazaki, J. Zmeskal, The asacusa antihydrogen and hydrogen program: results and prospects. Philos. Trans. Roy. Soc. A **376**(2116), 20170273 (2018). https://doi.org/10.1098/rsta.2017.0273

22. C.J. Baker, W. Bertsche, A. Capra, L.C.M. Charlton, A. Cridland Mathad, S. Eriksson, A. Evans, N. Evetts, S. Fabbri, J. Fajans, T. Friesen, M.C. Fujiwara, P. Grandemange, P. Granum, J.S. Hangst, M.E. Hayden, D. Hodgkinson, C.A. Isaac, M.A. Johnson, J.M. Jones, S.A. Jones, S. Jonsell, L. Kurchaninov, N. Madsen, D. Maxwell, J.T.K. McKenna, S. Menary, T. Momose, P. Mullan, K. Olchanski, A. Olin, J. Peszka, A. Powell, P. Pusa, C.Ø. Rasmussen, F. Robicheaux, R.L. Sacramento, M. Sameed, E. Sarid, D.M. Silveira, G. Stutter, C. So, T.D. Tharp, R.I. Thompson, D.P. van der Werf, J.S. Wurtele, Sympathetic cooling of positrons to cryogenic temperatures for antihydrogen production. Nat. Commun. **12**(1), 6139 (2021)
23. C.J. Baker, W. Bertsche, A. Capra, C.L. Cesar, M. Charlton, A.C. Mathad, S. Eriksson, A. Evans, N. Evetts, S. Fabbri, J. Fajans, T. Friesen, M.C. Fujiwara, P. Grandemange, P. Granum, J.S. Hangst, M.E. Hayden, D. Hodgkinson, C.A. Isaac, M.A. Johnson, J.M. Jones, S.A. Jones, S. Jonsell, L. Kurchaninov, N. Madsen, D. Maxwell, J.T.K. McKenna, S. Menary, T. Momose, P. Mullan, K. Olchanski, A. Olin, J. Peszka, A. Powell, P. Pusa, C.Ø. Rasmussen, F. Robicheaux, R.L. Sacramento, M. Sameed, E. Sarid, D.M. Silveira, G. Stutter, C. So, T.D. Tharp, R.I. Thompson, D.P. Werf, J.S. Wurtele, Sympathetic cooling of positrons to cryogenic temperatures for antihydrogen production. Nat. Commun. **12**(1), 6139 (2021). https://doi.org/10.1038/s41467-021-26086-1
24. C. Amsler, M. Antonello, A. Belov, G. Bonomi, R.S. Brusa, M. Caccia, A. Camper, R. Caravita, F. Castelli, P. Cheinet, D. Comparat, G. Consolati, A. Demetrio, L.D. Noto, M. Doser, M. Fanì, R. Ferragut, J. Fesel, S. Gerber, M. Giammarchi, A. Gligorova, L.T. Glöggler, F. Guatieri, S. Haider, A. Hinterberger, A. Kellerbauer, O. Khalidova, D. Krasnický, V. Lagomarsino, C. Malbrunot, S. Mariazzi, V. Matveev, S. Müller, G. Nebbia, P. Nedelec, L. Nowak, M. Oberthaler, E. Oswald, D. Pagano, L. Penasa, V. Petracek, L. Povolo, F. Prelz, M. Prevedelli, B. Rienäcker, O. Røhne, A. Rotondi, H. Sandaker, R. Santoro, G. Testera, I. Tietje, V. Toso, T. Wolz, P. Yzombard, C. Zimmer, N. Zurlo, Pulsed production of antihydrogen. Comm. Phys. **4**, 19 (2021). https://doi.org/10.1038/s42005-020-00494-z
25. E.K. Anderson, C.J. Baker, W. Bertsche, N.M. Bhatt, G. Bonomi, A. Capra, I. Carli, C.L. Cesar, M. Charlton, A. Christensen, R. Collister, A. Cridland Mathad, D. Duque Quiceno, S. Eriksson, A. Evans, N. Evetts, S. Fabbri, J. Fajans, A. Ferwerda, T. Friesen, M.C. Fujiwara, D.R. Gill, L.M. Golino, M.B. Gomes Gonçalves, P. Grandemange, P. Granum, J.S. Hangst, M.E. Hayden, D. Hodgkinson, E.D. Hunter, C.A. Isaac, A.J.U. Jimenez, M.A. Johnson, J.M. Jones, S.A. Jones, S. Jonsell, A. Khramov, N. Madsen, L. Martin, N. Massacret, D. Maxwell, J.T.K. McKenna, S. Menary, T. Momose, M. Mostamand, P.S. Mullan, J. Nauta, K. Olchanski, A.N. Oliveira, J. Peszka, A. Powell, C.Ø. Rasmussen, F. Robicheaux, R.L. Sacramento, M. Sameed, E. Sarid, J. Schoonwater, D.M. Silveira, J. Singh, G. Smith, C. So, S. Stracka, G. Stutter, T.D. Tharp, K.A. Thompson, R.I. Thompson, E. Thorpe-Woods, C. Torkzaban, M. Urioni, P. Woosaree, J.S. Wurtele, Observation of the effect of gravity on the motion of antimatter. Nature **621**(7980), 716–722 (2023). https://doi.org/10.1038/s41586-023-06527-1
26. V.A. Dzuba, V.V. Flambaum, G.F. Gribakin, W.A. King, Bound states of positrons and neutral atoms. Phys. Rev. A **52**(6), 4541 (1995). https://doi.org/10.1103/PhysRevA.52.4541
27. G.G. Ryzhikh, J. Mitroy, Positronic lithium, an electronically stable Li-$e^+$ ground state. Phys. Rev. Lett. **79**(21), 4124 (1997). https://doi.org/10.1103/PhysRevLett.79.4124
28. C. Harabati, V.A. Dzuba, V.V. Flambaum, Identification of atoms that can bind positrons. Phys. Rev. A **89**, 022517 (2014). https://doi.org/10.1103/PhysRevA.89.022517
29. V.V. Flambaum, C. Harabati, V.A. Dzuba, G.F. Gribakin, Periodic table of positronic atoms. J. Phys. Conf. Ser. **635**(5), 052028 (2015). https://doi.org/10.1088/1742-6596/635/5/052028
30. A.R. Swann, G.F. Gribakin, Model-potential calculations of positron binding, scattering, and annihilation for atoms and small molecules using a gaussian basis. Phys. Rev. A **101**, 022702 (2020). https://doi.org/10.1103/PhysRevA.101.022702
31. A.R. Swann, G.F. Gribakin, Positron binding and annihilation in alkane molecules. Phys. Rev. Lett. **123**, 113402 (2019). https://doi.org/10.1103/PhysRevLett.123.113402
32. J. Hofierka, B. Cunningham, C.M. Rawlins, C.H. Patterson, D.G. Green, Many-body theory of positron binding to polyatomic molecules. Nature **606**(7915), 688–693 (2022). https://doi.org/10.1038/s41586-022-04703-3
33. S.J. Gilbert, L.D. Barnes, J.P. Sullivan, C.M. Surko, Vibrational-resonance enhancement of positron annihilation in molecules. Phys. Rev. Lett. **88**, 043201 (2002). https://doi.org/10.1103/PhysRevLett.88.043201
34. J.R. Danielson, J.A. Young, C.M. Surko, Dependence of positron-molecule binding energies on molecular properties. J. Phys. B **42**, 235203 (2009). https://doi.org/10.1088/0953-4075/42/23/235203
35. J.R. Danielson, J.J. Gosselin, C.M. Surko, Dipole enhancement of positron binding to molecules. Phys. Rev. Lett. **104**, 233201 (2010). https://doi.org/10.1103/PhysRevLett.104.233201
36. J.R. Danielson, A.C.L. Jones, J.J. Gosselin, M.R. Natisin, C.M. Surko, Interplay between permanent dipole moments and polarizability in positron-molecule binding. Phys. Rev. A **85**, 022709 (2012). https://doi.org/10.1103/PhysRevA.85.022709
37. J.R. Danielson, A.C.L. Jones, M.R. Natisin, C.M. Surko, Comparisons of positron and electron binding to molecules. Phys. Rev. Lett. **109**, 113201 (2012). https://doi.org/10.1103/PhysRevLett.109.113201
38. A.R. Swann, G.F. Gribakin, J.R. Danielson, S. Ghosh, M.R. Natisin, C.M. Surko, Effect of chlorination on positron binding to hydrocarbons: experiment and theory. Phys. Rev. A **104**, 012813 (2021). https://doi.org/10.1103/PhysRevA.104.012813

39. J.R. Danielson, S. Ghosh, C.M. Surko, Influence of geometry on positron binding to molecules. J. Phys. B **54**(22), 225201 (2021). https://doi.org/10.1088/1361-6455/ac3e78
40. S. Ghosh, J.R. Danielson, C.M. Surko, Resonant annihilation and positron bound states in benzene. Phys. Rev. Lett. **129**, 123401 (2022). https://doi.org/10.1103/PhysRevLett.129.123401
41. J.R. Danielson, S. Ghosh, C.M. Surko, Enhancement of positron binding energy in molecules containing $\pi$ bonds. Phys. Rev. A **106**, 032811 (2022). https://doi.org/10.1103/PhysRevA.106.032811
42. J.P. Cassidy, J. Hofierka, B. Cunningham, C.M. Rawlins, C.H. Patterson, and D.G. Green, Many-body Theory Calculations of Positron Binding to Halogenated Hydrocarbons (2023)
43. C.M. Rawlins, J. Hofierka, B. Cunningham, C.H. Patterson, and D.G. Green, Many-body theory calculations of positron scattering and annihilation in H2, N2, and CH4 (2023) 2303.02083
44. J. P. Cassidy, J. Hofierka, B. Cunningham, D. G. Green; Many-body theory calculations of positronic-bonded molecular dianions. J. Chem. Phys. **160**(8), 084304 (2023). https://doi.org/10.1063/5.0188719
45. W.M. Haynes (ed.), *CRC Handbook of Chemistry and Physics*, 97th edn. (CRC Press, Boca Raton, 2016)
46. O.H. Crawford, Bound states of a charged particle in a dipole field. Proc. Phys. Soc. **91**, 279 (1967). https://doi.org/10.1088/0370-1328/91/2/303
47. H. Chojnacki, K. Strasburger, Configuration interaction study of the positronic hydrogen cyanide molecule. Mol. Phys. **104**, 2273 (2006). https://doi.org/10.1080/00268970600655477
48. M. Tachikawa, Y. Kita, R.J. Buenker, Bound states of the positron with nitrile species with a configuration interaction multi-component molecular orbital approach. Phys. Chem. Chem. Phys. **13**, 2701 (2011). https://doi.org/10.1039/C0CP01650K
49. Y. Kita, M. Tachikawa, Theoretical investigation of the binding of a positron to vibrational excited states of hydrogen cyanide molecule. Eur. Phys. J. D **68**(5), 116 (2014). https://doi.org/10.1140/epjd/e2014-40799-9
50. Y. Kita, R. Maezono, M. Tachikawa, M. Towler, R.J. Needs, Ab initio quantum Monte Carlo study of the positronic hydrogen cyanide molecule. J. Chem. Phys. **131**, 134310 (2009). https://doi.org/10.1063/1.3239502
51. A.R. Swann, G.F. Gribakin, Calculations of positron binding and annihilation in polyatomic molecules. J. Chem. Phys. **149**(24), 244305 (2018). https://doi.org/10.1063/1.5055724
52. J.S. Bell, E.J. Squires, A formal optical model. Phys. Rev. Lett. **3**(2), 96 (1959). https://doi.org/10.1103/PhysRevLett.3.96
53. W.H. Dickhoff, D.V. Neck, *Many-body Theory Exposed! - Propagator Description of Quantum Mechanics in Many-Body Systems*, 2nd edn. (World Scientific, Singapore, 2008)
54. A.L. Fetter, J.D. Walecka, *Quantum Theory of Many-particle Systems* (Dover, New York, 2003)
55. P. Ring, P. Schuck, *The Nuclear Many-Body Problem* (Springer, Berlin, 1980)
56. Y. Öhrn, *Propagators in Quantum Chemistry*, 2nd edn. (Wiley, Hoboken, New Jersey, 2004)
57. A. Dreuw, M. Head-Gordon, Single-reference ab initio methods for the calculation of excited states of large molecules. Chem. Rev. **105**(11), 4009 (2005). https://doi.org/10.1021/cr0505627
58. R.A. Kendall, T.H. Dunning Jr., R.J. Harrison, Electron affinities of the first-row atoms revisited systematic basis sets and wave functions. J. Chem. Phys. **96**(9), 6796–6806 (1992). https://doi.org/10.1063/1.462569
59. G.F. Gribakin, J. Ludlow, Many-body theory of positron-atom interactions. Phys. Rev. A **70**(3), 032720 (2004). https://doi.org/10.1103/PhysRevA.70.032720
60. D.G. Green, G.F. Gribakin, $\gamma$ spectra and enhancement factors for positron annihilation with core electrons. Phys. Rev. Lett. **114**, 093201 (2015). https://doi.org/10.1103/PhysRevLett.114.093201
61. D.G. Green, G.F. Gribakin, Enhancement factors for positron annihilation on valence and core orbitals of noble-gas atoms. Concepts, Methods and Applications of Quantum Systems in Chemistry and Physics. Prog. Theor. Chem. Phys. **31**, 243 (2018). https://doi.org/10.1007/978-3-319-74582-4_14
62. C.H. Patterson, Photoabsorption spectra of small Na clusters: TDHF and BSE versus CI and experiment. Phys. Rev. Mat. **3**, 043804 (2019). https://doi.org/10.1103/PhysRevMaterials.3.043804
63. C.H. Patterson, Density fitting in periodic systems: application to TDHF in diamond and oxides. J. Chem. Phys. **153**(6), 064107 (2020). https://doi.org/10.1063/5.0014106
64. H.-J. Werner, P.J. Knowles et al., The Molpro quantum chemistry package. J. Chem. Phys. **152**(14), 144107 (2020). https://doi.org/10.1063/5.0005081
65. F. Eckert, P. Pulay, H.-J. Werner, Ab initio geometry optimization for large molecules. J. Comput. Chem. **18**(12), 1473–1483 (1997)